Development of a ReaxFF reactive force field for intrinsic point defects in titanium dioxide

Reference:

Huygh Stijn, Bogaerts Annemie, van Duin Adri C.T., Neyts Erik.- *Development of a ReaxFF reactive force field for intrinsic point defects in titanium dioxide*

Computational materials science - ISSN 0927-0256 - 95(2014), p. 579-591

DOI: http://dx.doi.org/doi:10.1016/j.commatsci.2014.07.056

Development of a ReaxFF reactive force field for intrinsic point defects in Titanium Dioxide

Stijn Huygh[1,*], Annemie Bogaerts[1], Adri C. T. van Duin[2], Erik C. Neyts[1]

[1]Department of Chemistry, PLASMANT Research Group, University of Antwerp, Universiteitsplein 1, B-2610 Wilrijk-Antwerp, Belgium

[2]Department of Mechanical and Nuclear Engineering, Penn State University, University Park, Pennsylvania 16802, United States

*Corresponding author:

Tel: +32-3-265.23.46

Fax: +32-3-265.23.43

e-mail: stijn.huygh@uantwerpen.be

Abstract

A reactive ReaxFF force field is developed for studying the influence of intrinsic point defects on the chemistry with TiO_2 condensed phases. The force field parameters are optimized to ab initio data for the equations of state, relative phase stabilities for titanium and titanium dioxide, potential energy differences for $(TiO_2)_n$-clusters (n=1-16). Also data for intrinsic point defects in anatase were added. These data contain formation energies for interstitial titanium and oxygen vacancies, diffusion barriers of the oxygen vacancies and molecular oxygen adsorption on a reduced anatase (101) surface. Employing the resulting force field, we study the influence of concentration of oxygen vacancies and expansion or compression of an anatase surface on the diffusion of the oxygen vacancies. Also the barrier for oxygen diffusion in the subsurface region is evaluated using this force field. This diffusion barrier of 27.7 kcal/mol indicates that the lateral redistribution of oxygen vacancies on the surface and in the subsurface will be dominated by their diffusion in the subsurface, since both this barrier as well as the barriers for diffusion from the surface to the subsurface and vice versa (17.07 kcal/mol and 21.91 kcal/mol, respectively, as calculated with DFT), are significantly lower than for diffusion on the surface (61.12 kcal/mol as calculated with DFT).

Keywords:

Oxygen vacancy; interstitial titanium; oxygen diffusion; molecular dynamics; titanium dioxide; defects

1. Introduction

Titanium dioxide (TiO_2) is the natural occurring oxide of titanium, which exists in various polymorphs. The three most stable polymorphs are rutile, anatase and brookite, in that order of abundance. Thanks to its high reactivity, anatase is widely applied in photocatalysis [1] and solar energy conversion [2]. Especially the surface is critically important for these applications, and for this reason the interest in the chemical and physical properties of the surfaces has increased significantly in the past decades. The reader is referred to a review [3] for a summary of the research on TiO_2 surfaces.

The higher catalytic activity of anatase with respect to rutile is due to the behaviour of its intrinsic point defects. It is indeed well known that point defects strongly affect the physical and chemical properties of metal oxides. In heterogeneous catalysis the defect sites act as an initiator for adsorption of molecules and/or metal particles. In photocatalysis the defects influence the surface reactivity, either favourably or detrimentally. A favourable effect occurs when oxygen vacancies act as trap sites for photoexcited charge carriers such that these carriers are transported to the surface. A detrimental effect occurs when these oxygen vacancies act as recombination centers for these carriers which will lower the reactivity. Not only the “chemistry” is influenced significantly by these defects, but the diffusion of point defects also plays a key role in the mass transport between the surface and the bulk during surface preparation techniques such as annealing or sputtering. [4]

The location of the defect determines its role and its properties. Density functional theory (DFT) calculations demonstrated that for an anatase (101) surface, which is the lowest energy and most exposed surface, [5,6] the subsurface oxygen vacancies are 0.5 eV more stable than surface vacancies. [7] The diffusion barriers of these defects from the surface region to the

subsurface region are around 1 eV. [7] This indicates that surface oxygen vacancies, once formed, diffuse relatively easily to the subsurface, which is consistent with the low density of surface defects found experimentally with scanning tunneling microscopy (STM) [8,9] and the high density of O vacancies indicated by ultraviolet photoemission spectroscopy (UPS) [10] that also accesses the subsurface region. Therefore, the subsurface oxygen vacancies will play a more prominent role than the surface vacancies; this is in contrast with rutile where the opposite trend is observed, both theoretically [4] as well as experimentally with STM [8,9] and UPS [10]. Because of the differences in these trends, anatase has a higher catalytic activity than rutile. The subsurface defects have a longer lifetime than surface defects, because the latter will be quenched by molecules in the environment.

Because of the accuracy and speed of modern quantum mechanical (QM) methods, they can be used to calculate the energy and the geometry of molecules and solid state systems. Ab initio MD has also been extensively used to model dynamical processes of relatively large molecules adsorbed on solid state substrates. However to reach larger time and space scales, classical molecular dynamics simulations may be used as a complimentary technique. In this work, we developed a classical reactive force field for titanium dioxide for the ReaxFF method developed by van Duin and coworkers [11]. The main focus of this force field is the correct description of intrinsic point defects, oxygen vacancies and titanium interstitials in anatase. The developed force field thus allows larger spatial scale and longer time scale simulations of the titanium dioxide system compared to DFT, with comparable accuracy. For instance, in the LAMMPS implementation of ReaxFF [12], it is possible to simulate systems with 10^6 atoms at nanosecond timescales. [13,14,15,16] Within LAMMPS there is also another variable-charge reactive force field implemented, namely the charge-optimized many-body potential (COMB) developed by

Sinnott, Phillpot and coworkers. [17,18,19,20,21,22] Also for COMB a parametrization for the titanium dioxide system has been developed. [23]

2. Computational Methods

2.1 ReaxFF

ReaxFF is a generic bond order dependent force field. In this method the forces are derived from the following energy expression:

$$E_{system} = E_{bond} + E_{over} + E_{under} + E_{lp} + E_{val} + E_{vdWaals} + E_{coulomb}$$

The energy expression for the system consists of different partial contributions: bond energies (E_{bond}), energy penalties for over-coordination (E_{over}) and (optionally) stabilize under-coordination of atoms (E_{over} and E_{under}), lone-pair energies (E_{lp}), valence angle energies (E_{val}) and terms to handle non-bonded van der Waals ($E_{vdWaals}$) and Coulomb ($E_{coulomb}$) interaction energies. All terms except the non-bonding terms include a bond-order dependence and depend on the local environment of each atom. Bond-orders are determined by a general relation between interatomic distance and bond-order. The bond-order dependence is generated by an expression of which the parameters are fitted to a large database of structures and energies as described below. With this expression the bond-order is calculated throughout the MD-simulation determined by the instantaneous interatomic distances. ReaxFF is capable of describing charge transfer in chemical reactions. This is possible because the Coulomb energy ($E_{coulomb}$) is calculated by using a geometry dependent charge distribution determined using the

electronegativity equalization method (EEM) [24]. The individual atomic charges are calculated in each time step of the MD-simulation. Short-range Pauli repulsion and long-range dispersion are included in the van der Waals energy term ($E_{vdWaals}$). A more detailed description of the ReaxFF method can be found in van Duin et al. [11] and Chenoweth et al. [25]. This Ti-O force field has the same O atomic parameters and O/H pair parameters as recently published ReaxFF descriptions for Zn/O/H [26], Fe/O/H [27], Si/O/H [28], proteins [29], Ti/O/H [30,31,32] making it straightforward to integrate these potentials. All mentioned force fields have the same O atomic parameters and O/H pair parameters. Only the Ti/H, Ti-O-H, O-Ti-O-H and Ti-O-O-H interactions thus need to be included in a further fitting to expand this force field to Ti/O/H. As best available initial guess for the development of a force field that describes the influence of intrinsic point defects on the chemistry of TiO_2, the Ti/O/H force field developed by Kim and co-workers [31,32] was used. In the future, the force field as developed in this paper, describing the chemistry of the intrinsic point defects, will be expanded to the interaction of water and organic molecules with reduced surfaces.

2.2 Training set

In this work the force field parameters for the TiO_2-system have been re-evaluated, starting from the ReaxFF Ti/O parameters, as developed earlier by Kim and co-workers [30,31,32], but refocusing the training on intrinsic point defects, which were previously not considered. The training set consists of a set of QM and some experimental data. This data is taken from literature, the QM level and some of the computational details are given between parentheses after the description of the data points added to the training set. For the equations of state (EOS)

of titanium dioxide, required for an adequate description of volume-energy relations, approximately 10 data points for each of the 8 TiO_2 polymorphs (anatase, rutile, brookite, columbite, baddeleyite, pyrite, fluorite and cottunite), are added to the training set with an increment of about 2% increase or decrease in volume. (All polymorphs except brookite: LCAO-HF-TVAE* [33], brookite: DFT-B3LYP-6-31G [22]) The QM results indicate that anatase is more stable than rutile while the experiment indicates otherwise, and therefore the cohesive energy differences of anatase, rutile and brookite are taken from experiment [35]. The five high energy polymorphs are not important for the final result, even though they are not very accurate. To match the corresponding geometry of each data point, the unit cell of each phase is expanded or contracted within the ReaxFF calculation.

For the three most abundant phases of titanium dioxide, i.e., rutile, anatase and brookite, the heats of formation were used. [36] Also potential energy differences of 30 $(TiO_2)_x$-clusters (x=1-16) are added. [30,37,38,39] (DFT-B3LYP, LACVP**)

For the anatase (101) surface the formation energies of oxygen vacancies at the surface and in the subsurface [7,40] (DFT-GGA PBE, Γ-point, spin restricted), the diffusion barriers of these vacancies [7,40] (DFT-GGA PBE, 2x2x1 k-point mesh, spin restricted, NEB), the formation energies of interstitial titanium [40] (DFT-GGA PBE, Γ-point, spin restricted) and the oxygen adsorption energies at the reduced surface [41] (DFT-GGA PBE, Γ-point, spin unrestricted) are added to the training set.

2.3 Force field fitting

The force field parameters were fitted to the training set containing all the data points mentioned in the previous section. The parameters that were adjusted are the Ti atomic parameters, the Ti-Ti, Ti-O and O-O bond parameters and the O-Ti-O, Ti-O-Ti, Ti-O-Ti, Ti-O-O and Ti-Ti-O valance angle parameters.

To find the most optimal set of parameters a sequential one-parameter search [30] has been used to minimize the sum-of-squares error function:

$$\text{Error} = \sum_{i}^{n} \left[\frac{(x_{i,QM} - x_{i,ReaxFF})}{\sigma_i} \right]^2$$

In this equation $x_{i,QM}$ is the QM value in the training set, $x_{i,ReaxFF}$ is the ReaxFF calculated value and σ_i is the weight assigned to data point i. In total around 270 data points were added and 240 corresponding structures were used in the force field fitting. The sequential one-parameter search method has been performed in multiple cycles of 88 adjusted parameters to account for parameter correlation [11]. The result of the force field fitting and a comparison between the training set, reference QM data, and the ReaxFF calculated data are presented below.

3. Results and Discussion

In this section we will compare the ReaxFF calculated data, the data added to the training set and the data as calculated with other ReaxFF force fields [30,31,32]. These data consist of the equations-of-state, relative phase stabilities, TiO_2-cluster stabilities, formation energies of interstitial titanium and oxygen vacancies, diffusion barriers of the oxygen vacancies and oxygen adsorption energies on a reduced anatase (101) surface. This comparison between the data as

calculated with the currently developed force field, two other force fields and the data which was included in the training set is discussed in subsections 3.1 – 3.4. Also subsurface diffusion and the influence of defect concentration and compressing or expanding the anatase (101) surface on the oxygen vacancies diffusion barriers will be presented in subsection 3.5; this subsection contains only data as obtained with the force field developed in this article.

In the further discussion the current developed ReaxFF force field parameterization is simply indicated as “ReaxFF”. If Kim is mentioned the ReaxFF force field as published in reference [30] is meant, and when Monti is mentioned the ReaxFF force field as published in references [31] and [32] is meant.

3.1 Equations of state (EOS) and Relative phase stability

Figure 1 shows the cohesive energy differences between the different titanium dioxide polymorphs relative to rutile. ReaxFF predicts that anatase is more stable than rutile, which is inconsistent with the experimental data where an energy difference is found of 0.62 kcal/mol [35]. The stability, however, is dependent on the surface area, and for larger surface areas anatase becomes indeed more stable than rutile. [43] The value used by Levchenko et al. [44] and Smith et al. [45] is 0.4 ± 0.1 kcal/mol with rutile the most stable polymorph. For such a small difference it is not surprising that the ReaxFF force field does not reproduce the correct energy difference. Since phase transitions in solid phases lay far beyond the time scale typically attainable in MD simulations, this will, however, not cause problems. The cohesive energy differences for the four most stable phases (rutile, anatase, brookite and columbite) are correct within 1.6 kcal/mol. The

four higher energy phases, which are not important for this force field, show discrepancies up to 8 kcal/mol, although the correct stability order is preserved.

The Kim and Monti force fields reproduce the cohesive energy differences of TiO_2 within 1.8 and 2.1 kcal/mol, respectively. In case of the Kim force field the order of the relative stabilities for the most stable phases is correct. The Monti force field, on the other hand, predicts the anatase phase to be less stable than rutile, which is consistent with the experimental data, but more stable than brookite, which is inconsistent with the experimental data. This means that the trends in the other force fields are comparable to or slightly better than those in the current force field, but since phase transitions lay beyond the typical time scale of MD simulations, this will not cause problems during simulations.

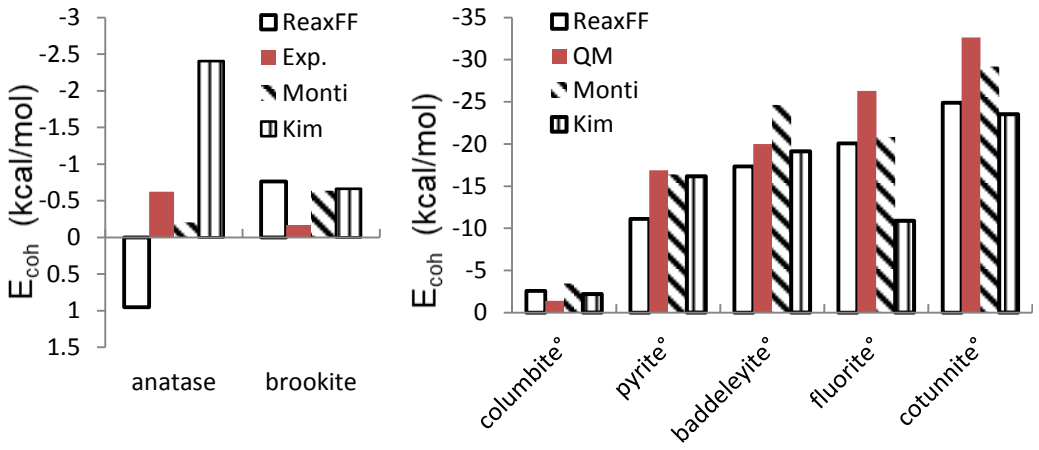

Figure 1: Energy differences between different TiO_2 polymorphs relative to rutile. The experimental data are from reference [35] and the QM data from reference [33].

Figures 2, 3 and 4 show the EOS of the three most abundant TiO_2 polymorphs, i.e., rutile, anatase and brookite, respectively.

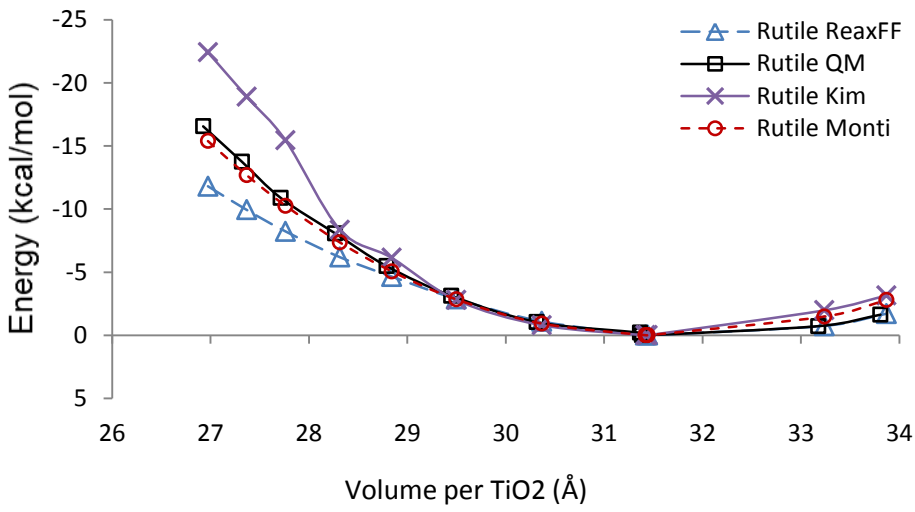

Figure 2: Comparison of the EOS of rutile calculated with ReaxFF, QM[33], Monti and Kim.

The volume-energy relationship in ReaxFF describes the expansion of rutile very well, but when compressing the structure the error increases gradually up to 4.75 kcal/mol (28.6% error) when the volume is reduced with 15%. The three force fields reproduce similar equations of state. The Monti force field reproduces the compression in a better way, while the Kim force field performs worse when compression occurs.

The volume-energy relationship of anatase is described very well overall, showing a maximum discrepancy of 0.81 kcal/mol (11.7% error) for a compression of 10%, while an error of only 0.65 kcal/mol (11.26% error) is found when the volume is expanded with 11%. This accurate description of the volume-energy relationship of anatase thus demonstrates the reliability of the force field with respect to a description of pressure effects on the chemistry of anatase. In the case of the Monti and Kim force fields the minimum is (incorrectly) shifted to lower volumes and the shape of the curve differs from the QM one. The Kim force field gives a curve which is a

bit too narrow and Monti generates a curve which is too flat in the case of compression, corresponding to force constant which is too high and too low, respectively. Overall, however, all three force fields are in decent agreement with the QM data.

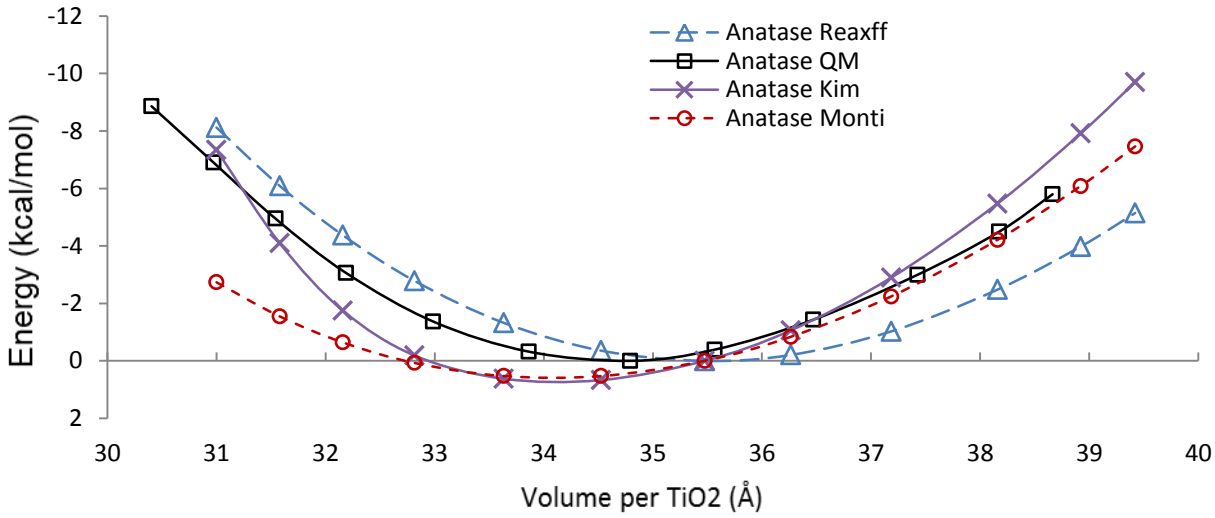

Figure 3: Comparison of the EOS of anatase calculated with ReaxFF QM[33], Monti and Kim.

Finally, also the EOS of brookite is described well, with the error gradually increasing up to 3 kcal/mol (24.7% error) when the volume is reduced with 14%. The force fields of Kim and of Monti have errors within the same order of magnitude.

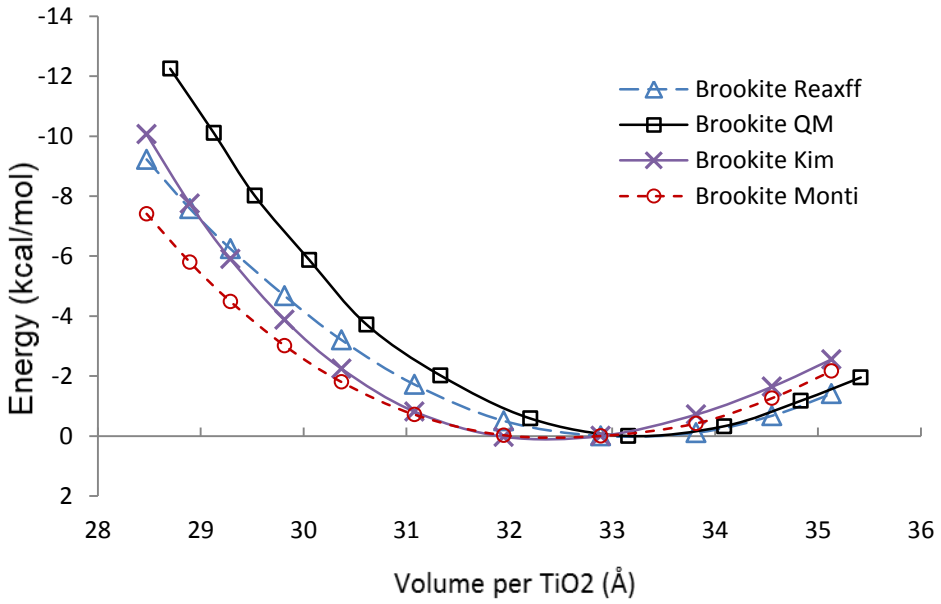

Figure 4: Comparison of the EOS of brookite calculated with ReaxFF, QM[22], Monti and Kim.

In Table 1 the lattice parameters as calculated with QM methods and ReaxFF are compared with the experimental values. As can be seen by the percentile deviations between the calculated and measured values, the currently developed force field overestimates the lattice parameters in all cases. The QM methods underestimate the a/b lattice value of rutile and anatase, and overestimate all other lattice parameters. The overestimation of the lattice parameters by ReaxFF is the same for all lattice parameters of the same polymorph of titanium dioxide. This means that the crystal structure is expanded equally in every direction in comparison with the experiments.

Table 1. Lattice parameters of rutile, anatase and brookite as calculated with QM methods and ReaxFF and as measured in the experiments. The values between the parentheses are the percentile deviations in comparison with the experiment.

Method	a	b	c
		Rutile	
HF-TVAE* [33]		4.575 (-0.26)	2.999 (1.52)
ReaxFF		4.605 (0.39)	2.966 (0.41)
Exp. [33]		4.587	2.954
		Anatase	
HF-TVAE*[33]		3.781 (-0.03)	9.735 (2.45)
ReaxFF		3.837 (1.45)	9.639 (1.44)
Exp. [33]		3.782	9.502
		Brookite	
B3LYP-6-31G [22]	9.276 (1.00)	5.502 (1.00)	5.197 (1.01)
ReaxFF	9.252 (0.74)	5.487 (0.73)	5.183 (0.74)
Exp. [34]	9.184	5.447	5.145

3.2 TiO_2 clusters

To ensure that the developed force field is able to describe the influence of structure and size on the potential energy per TiO_2 unit, 30 TiO_2 cluster structures of the type $(TiO_2)_n$ with n equal to 1-16 were added to the training set for the force field fitting. Figure 5 shows the comparison of the results obtained with ReaxFF, DFT and the Monti and Kim force fields for the potential energy difference of 29 different $(TiO_2)_n$ cluster configurations divided by n, the number of TiO_2 units, with the $(TiO_2)_{16}$ potential energy divided by 16 taken as reference point. The different structures are depicted in figure 6. A reasonable agreement with the QM data [30,37,38,39] is found for the smaller cluster sizes up to 4, and the error converges for the larger clusters. The data produced by Kim's force field is in very good agreement with the QM data, while Monti's

force field gives results for which the agreement is in between the currently developed force field and the one from Kim. The discrepancy between ReaxFF and QM decreases with increasing cluster size, which is a clear indication that large-scale simulations for TiO_2 will be accurate. "The larger discrepancies with ReaxFF between the relative stabilities for the smaller cluster sizes up to $(TiO_2)_4$ are caused by the oxygen atoms which are only bonded to one titanium atom; this type of oxygen atom is not found in the larger cluster sizes. The Ti-O bond lengths for this type of oxygen atom are found to be ~13.5% too short compared to the QM data, while the bond lengths for this type of oxygen are found to be too short; the other Ti-O bond lengths are almost identical in ReaxFF compared to DFT."

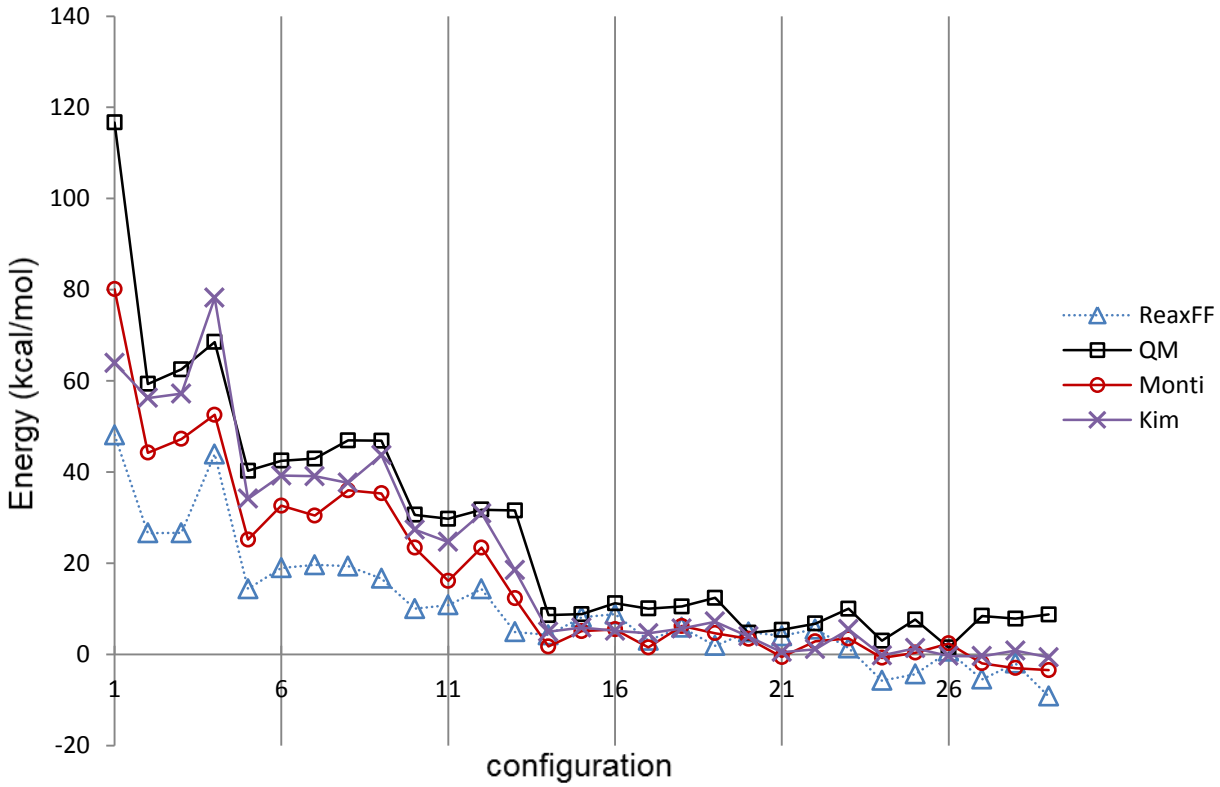

Figure 5: Potential energy difference between the different configurations (see figure 6) and the reference structure (i.e., $(TiO_2)_{16}$)[30,37,38,39]

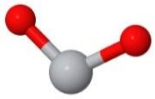

TiO_2 (1)

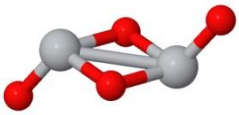

$(TiO_2)_2$ type I (2)

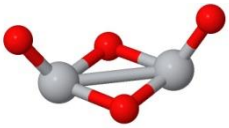

$(TiO_2)_2$ type II (3)

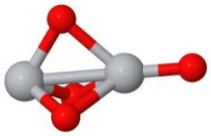

$(TiO_2)_2$ type III (4)

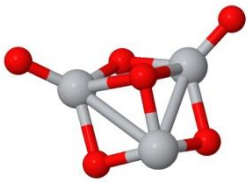

$(TiO_2)_3$ type I (5)

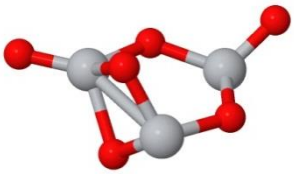

$(TiO_2)_3$ type II (6)

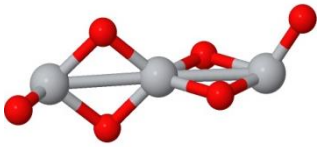

$(TiO_2)_3$ type III (7)

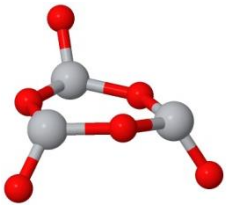

$(TiO_2)_3$ type IV (8)

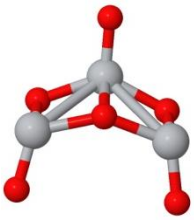

$(TiO_2)_3$ type V (9)

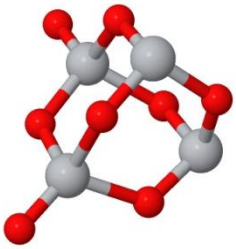

$(TiO_2)_4$ type I (10)

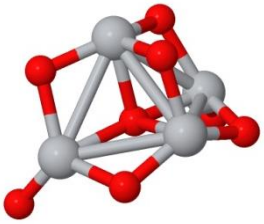

$(TiO_2)_4$ type II (11)

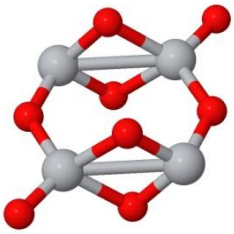

$(TiO_2)_4$ type III (12)

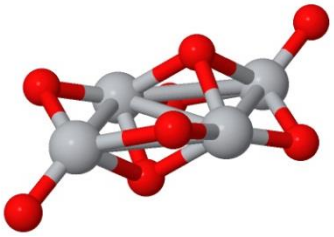

$(TiO_2)_4$ type IV (13)

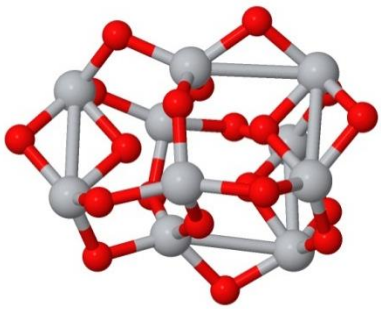

$(TiO_2)_{10}$ type I (14)

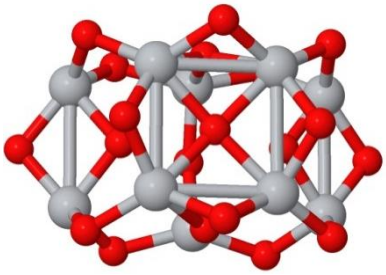

$(TiO_2)_{10}$ type II (15)

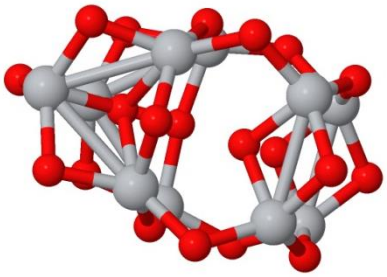

$(TiO_2)_{10}$ type III (16)

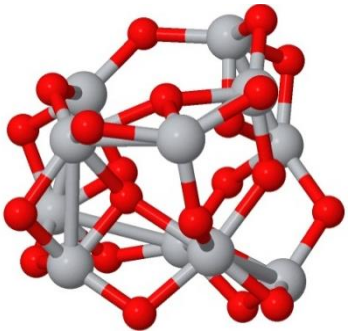

$(TiO_2)_{11}$ type I (17)

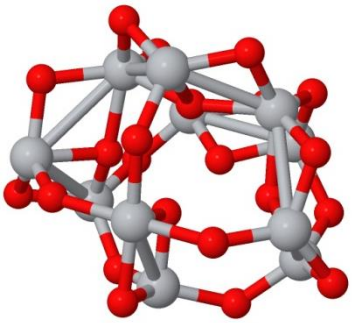

$(TiO_2)_{11}$ type II (18)

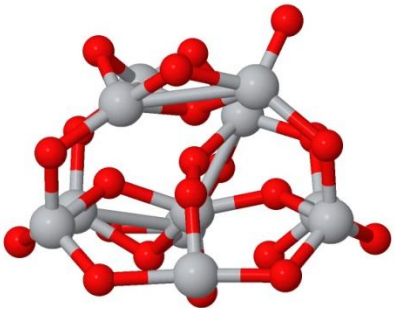

$(TiO_2)_{11}$ type III (19)

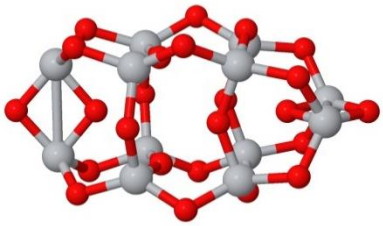

$(TiO_2)_{12}$ type I (20)

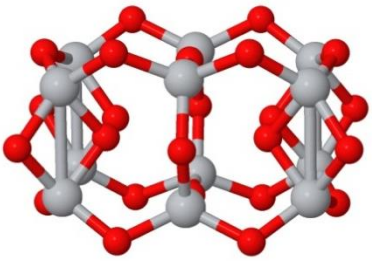

$(TiO_2)_{12}$ type II (21)

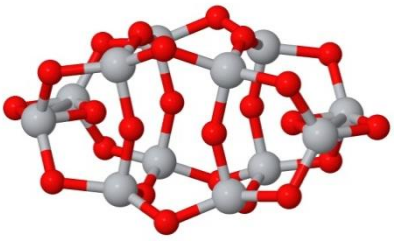

$(TiO_2)_{12}$ type III (22)

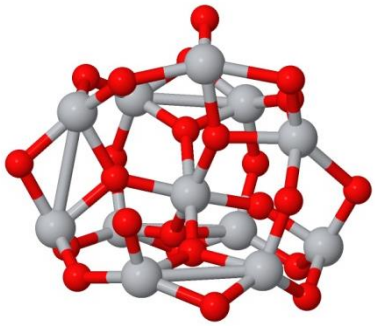

$(TiO_2)_{12}$ type IV (23)

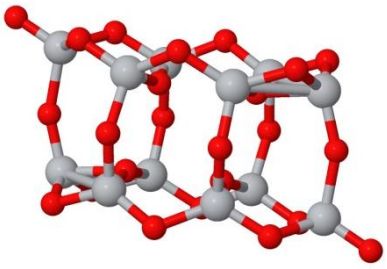

$(TiO_2)_{12}$ type V (24)

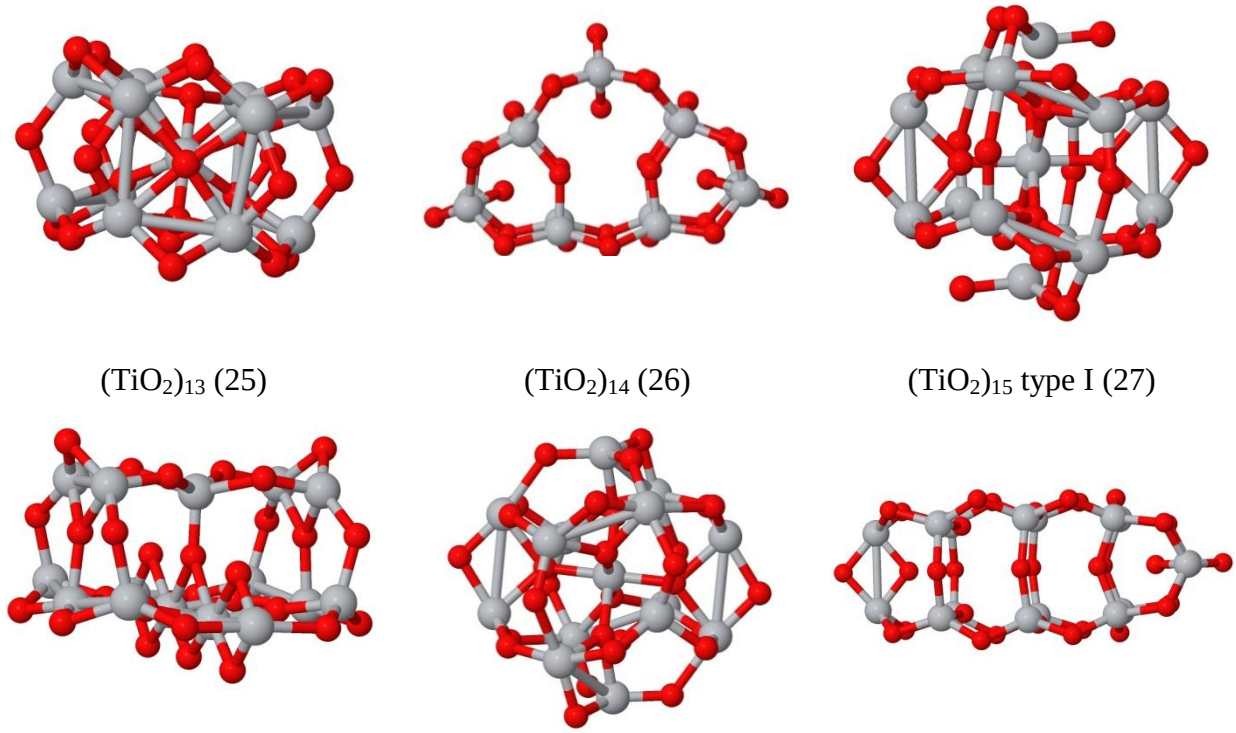

$(TiO_2)_{13}$ (25) $(TiO_2)_{14}$ (26) $(TiO_2)_{15}$ type I (27)

$(TiO_2)_{15}$ type II (28) $(TiO_2)_{15}$ type III (29) $(TiO_2)_{16}$ (30)

Figure 6: The DFT optimized configurations of the TiO_2 clusters (Ti = gray, O = red (dark gray))

3.3 Point defects

Point defects play an important role in the surface chemistry of metal oxides like titanium dioxide. They can act as centers where molecules can adsorb. For instance, molecular oxygen will not adsorb on a stoichiometric anatase (101) surface, but it will adsorb when an oxygen vacancy is present in the subsurface. [41] An important feature of anatase (101) is the distribution of oxygen vacancies in the surface and the subsurface, as this distribution determines the catalytic superiority of anatase compared to rutile. [40] There are more subsurface vacancies

present in anatase than surface vacancies because of the lower formation energy and thus higher stability and the low (around 1 eV) diffusion barriers. The opposite trend is found for rutile. [7,40] Because of this clear importance of the point defects on the surface chemistry of anatase, data for these defects were added to the training set as well. These data consist of oxygen vacancy formation energies, diffusion barriers for oxygen vacancies, interstitial titanium formation energies and adsorption energies of molecular oxygen at a reduced anatase (101) surface.

3.3.a Interstitial titanium

In Figure 8 the formation energies of interstitial titanium are shown, calculated with the new force field, with DFT [40] and with the force fields of Monti and Kim. T1-T6 represent the different locations where the interstitial titanium atom can occur in an anatase (101) surface composed of 72 atoms, corresponding to 3 atomic layers. The positions of T1-T6 are shown in Figure 7. The nomenclature is the same as in reference 40. T2 is not shown because this was found not to be stable during the minimization, which is consistent with the diffusion energy barrier from T2 to T1 to be 0 kcal/mol as calculated with DFT [40]. ReaxFF underestimates all formation energies compared to the DFT result, especially for T1, for which the formation energy calculated with ReaxFF lies 9.5% below the value calculated with DFT [40]. This means that ReaxFF overestimates the significance of T1 in comparison with T3 and T4. More importantly, however, ReaxFF correctly predicts the T5 and T6 to be the most stable ones. This is specifically important for the defect distribution, since this distribution depends on the difference in formation energies between the different sites. The force fields of Kim and of

Monti yield the same trends as found with the currently developed force field, but the formation energies as found with these force fields are about an order of magnitude off, such that the formation of interstitial titanium defects will occur too easily and therefore the concentration of these defects would be too high. The formation energies of interstitial titanium as calculated with DFT and ReaxFF are approximately twice the values of the formation energies of the oxygen vacancies, so they are of less importance for the surface chemistry. The higher formation energies of interstitial titanium compared to oxygen vacancies also directly correlate with their lower stability, which might cause a higher reactivity of the surface. In a theoretical study [46] concerning the influence of subsurface defects on the water adsorption and dissociation of water on an anatase (101) stoichiometric and reduced surface, it is found that both interstitial titanium and oxygen vacancies increase the adsorption energy of adsorbed water in the vicinity of these defects. The energy barrier for the dissociation of water is decreased from 12.91 kcal/mol on the stoichiometric surface to 5.53 kcal/mol and 6.00 kcal/mol, for an anatase (101) surface with an interstitial titanium and a surface with an oxygen vacancy present, respectively. At one adsorption site in the case of an interstitial titanium present, the dissociation of water is found to be exothermic. In contrast, in all other cases the dissociation is found to be endothermic. Another theoretical study [47], which is focused on the adsorption and dissociation of CO_2 on an anatase (101) stoichiometric and reduced surface, indicates that interstitial titanium and oxygen vacancies increase the adsorption energies of CO_2 in comparison with the stoichiometric anatase (101) surface. For the most stable CO_2 adsorption configurations the energy barriers of dissociation are 20.8 kcal/mol and 17.5 kcal/mol for surfaces with an oxygen vacancy and interstitial titanium present, respectively. Interstitial titanium seems to increase the adsorption energies and decrease the energy barriers for dissociation of water and CO_2 more than oxygen

vacancies, but these differences are within reasonable level. They do play a role, however, for the mass transport occurring between the surface and the bulk when the structure is annealed, [4] due to their particularly low diffusion barriers (less than 0.5 eV). [40]

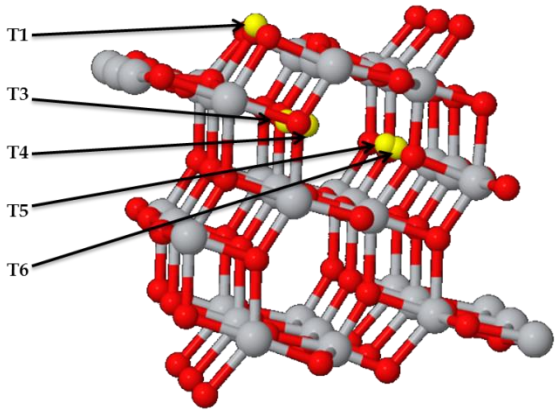

Figure 7: Different positions for interstitial titanium in the anatase (101) surface. (Ti = gray, $Ti_{interstitial}$ = yellow (light gray), O = red (dark gray))

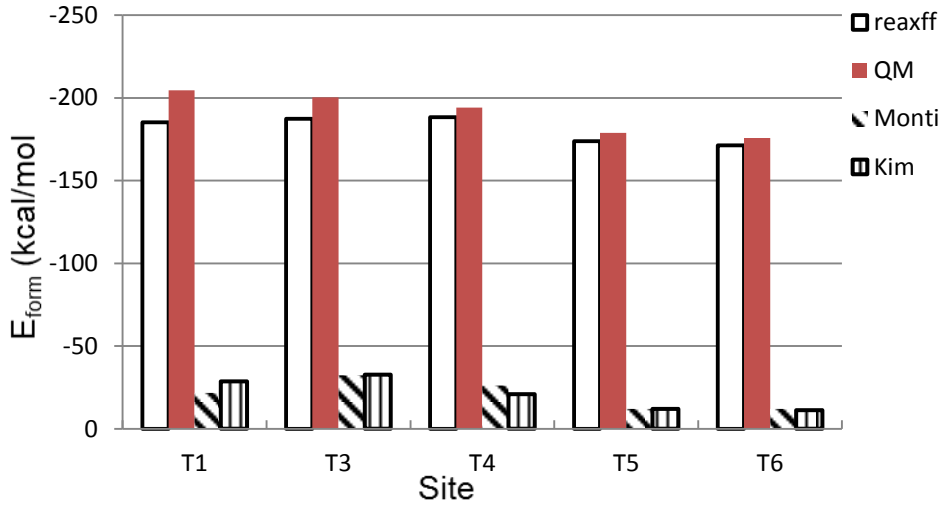

Figure 8: Formation energies calculated with ReaxFF, DFT [40], Monti and Kim for the different interstitial titanium sites located in the anatase (101) surface (see figure 7)

The diffusion pathways of the interstitial titanium [40] were not used during the fitting of the current force field. The comparison between the values calculated with ReaxFF and with DFT [40] are given in Table 2. The errors on the ReaxFF values are large, so it is advisable to not use the currently developed force field for reactions where the diffusion of the interstitial titanium might be important. In the case of migration from site T3 to T4 and T5 to T6 the discrepancies are reasonable so that the diffusion still might occur at room temperature. For reactions where the diffusion is not part of the reaction mechanism the force field will be able to reproduce the mechanism as long as the interstitial titanium defect was present at the desired site.

Table 2: Diffusion barriers for interstitial in anatase (101) as calculated with ReaxFF and DFT[40].

Pathway	Direct pathway		Reverse pathway	
	$E_{a,ReaxFF}$ (kcal/mol)	$E_{a,QM}$ (kcal/mol)	$E_{a,ReaxFF}$ (kcal/mol)	$E_{a,QM}$ (kcal/mol)
T1-T3	76.10	8.99	73.56	13.14
T3-T4	8.76	3.23	8.07	9.45
T4-T5	44.28	10.61	61.11	25.83
T5-T6	8.99	0.92	8.07	4.38

3.3.b Oxygen vacancies

In figure 10 the formation energies for oxygen vacancies in three different anatase (101) surfaces are shown, calculated with the new force field, with DFT [7,40] and with the force fields of Monti and Kim. The structure containing 216 atoms (corresponding to the stoichiometric structure) consists of 6 atomic layers, while the structures containing 72 and 108 atoms consist of 3 atomic layers. These different structures are all used in the training set to

account for the increasing stability of subsurface vacancies relative to the surface vacancies for increasing slab thickness [40]. This is caused by the fact that the surface is more rigid than the subsurface, as indicated by the analysis of the structural relaxations around the vacancy sites, which shows larger atomic displacements in the subsurface region than at the surface. [40] If the structure size increases there will be more possibilities to relax if a vacancy is formed in the subsurface then when one is formed at the surface. Nomenclature can be found on figure 9 and is the same as in reference [40]. V_{O1}, V_{O2} and V_{O3} are surface oxygen vacancies of which V_{O1} has the lowest formation energy and therefore will be the most abundant. V_{O4} and V_{O5} are subsurface vacancies which have a considerably lower formation energy, $\Delta E \approx 11.5$ kcal/mol, than that of V_{O1}, so they will play a more prominent role in the surface chemistry of anatase. The relative probability of formation of a surface vacancy V_O with respect to subsurface sites is $\sim 4 \times 10^{-9}$ and $\sim 1.6 \times 10^{-3}$ at T = 300 K and 900 K, respectively. The QM values for V_{O4} and V_{O5} are almost identical, i.e., 85.09 and 84.17 kcal/mol, respectively, and they are almost identical to the bulk V_O formation energy, which is 85.09 kcal/mol (as calculated with only the Γ-point), so V_{O4} and V_{O5} can be considered "bulk-like" [7,40].

The values and the trends for the formation energies of V_O are reproduced well for such an extensive data set that describes different influences on the formation energies. The root mean square error on the energy is 4.08 kcal/mol. A few rather large discrepancies, up to 9.4% for the least stable surface vacancies, V_{O2}, occur, while good agreement for V_{O1} and V_{O4} is obtained for which the root mean square error is 1.98 kcal/mol and 2.50 kcal/mol, respectively. The QM bulk oxygen vacancy formation energy is 101.70 kcal/mol (2x2x2 k-point mesh) [40] and 85.09 kcal/mol (Γ-point) [40], in comparison the ReaxFF value of 95.89 kcal/mol, which is close to the average between both QM values. For Kims and Monti's force field the V_{O1} formation energy is

lower than that of the subsurface vacancy sites. This is opposite to the trend shown by the DFT data. This fact, together with the fact that the errors for the oxygen vacancy formation energies of the two force fields are about one order of magnitude off, makes that these force fields not capable of accurately describing the differences between the different oxygen vacancies. Because of these large discrepancies in absolute numbers and trends the oxygen vacancy diffusion barriers were not calculated for these two force fields.

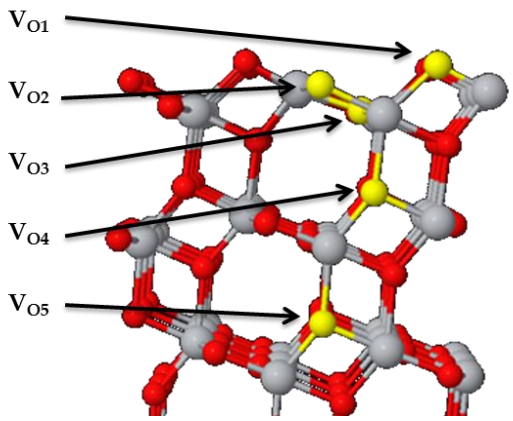

Figure 9: Different oxygen vacancy sites in anatase (101)

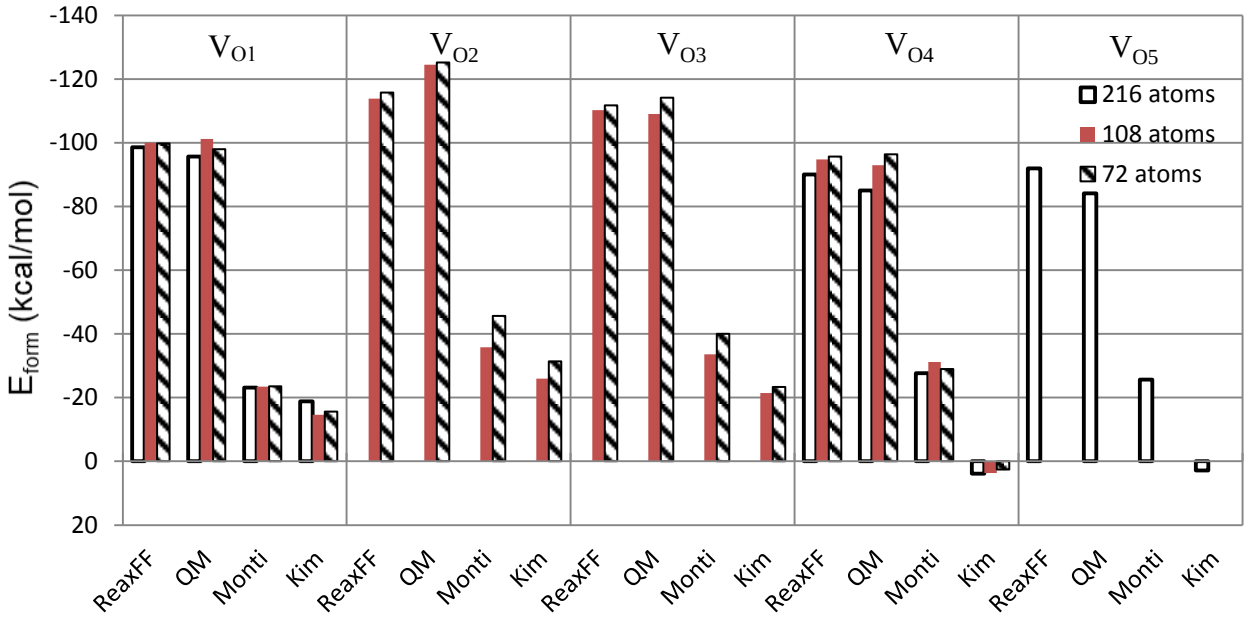

Figure 10: Oxygen vacancy formation energies calculated with ReaxFF, DFT[7,40], Monti and Kim for the different anatase (101) surfaces (216 atoms (6 atom layers), 108 and 72 atoms (3 atom layers)

The diffusion barriers of the oxygen vacancies in anatase (101), as calculated with ReaxFF and with DFT [7,40], can be found in Table 3. The barriers were calculated using Nudged Elastic Band [50]. These are the diffusion barriers for the anatase (101) surface consisting of 72 atoms and 3 atomic layers. Note that for the $V_{O1} \rightarrow V_{O4}$ pathway the diffusion barrier for the reverse pathway will be higher for a structure with for example 6 atomic layers. This is caused by the stabilisation of V_{O4} relative to V_{O1} because of the increasing possibilities to relax the perturbation. Only the unique and the lowest pathways were added to the training set. For example, the lowest energy pathway $V_{O1} \rightarrow V_{O2}$ consists of a combination of $V_{O1} \rightarrow V_{O3}$ and $V_{O3} \rightarrow V_{O2}$.

The barriers and the trends in the barriers are described quite well by our force field. Especially the most important pathway, $V_{O1} \rightarrow V_{O4}$, is described very well with a maximum error of 0.5 kcal/mol. Only the diffusion between V_{O2} and V_{O3} shows larger discrepancies which is caused by the large error in the relative stability of V_{O2}. This, however, is of less importance because especially the distribution between the surface and subsurface vacancies will influence the surface chemistry and reactivity. The pathway of $V_{O1} \rightarrow V_{O4}$ is shown in figure 11. This pathway consists of two atoms moving simultaneously. Vacancy diffusion on the surface is largely inhibited, particularly the $V_{O1} \rightarrow V_{O1`}$ diffusion along [010], which has a barrier of 61.12 kcal/mol as calculated with DFT [40]. The $V_{O1} \rightarrow V_{O1`}$ diffusion pathway is shown in figure 12.

Table 3: Diffusion barriers for oxygen vacancies in anatase (101) as calculated with ReaxFF and DFT [7,40].

Pathway	**Direct pathway**		**Reverse pathway**		**Diffusion direction**
	$E_{a,ReaxFF}$ (kcal/mol)	$E_{a,QM}$ (kcal/mol)	$E_{a,ReaxFF}$ (kcal/mol)	$E_{a,QM}$ (kcal/mol)	
$V_{O1} \rightarrow V_{O1'}$	79.6	61.12	79.6	61.12	[010]
$V_{O1} \rightarrow V_{O3}$	34.7	30.90	22.9	17.99	$[66\bar{1}]$
$V_{O1} \rightarrow V_{O4}$	17.2	17.07	21.4	21.91	$[301]+[30\bar{1}]$
$V_{O2} \rightarrow V_{O3}$	7.2	6.92	11.2	17.99	[031]
$V_{O3} \rightarrow V_{O4}$	20.2	17.99	36.3	35.98	[661]

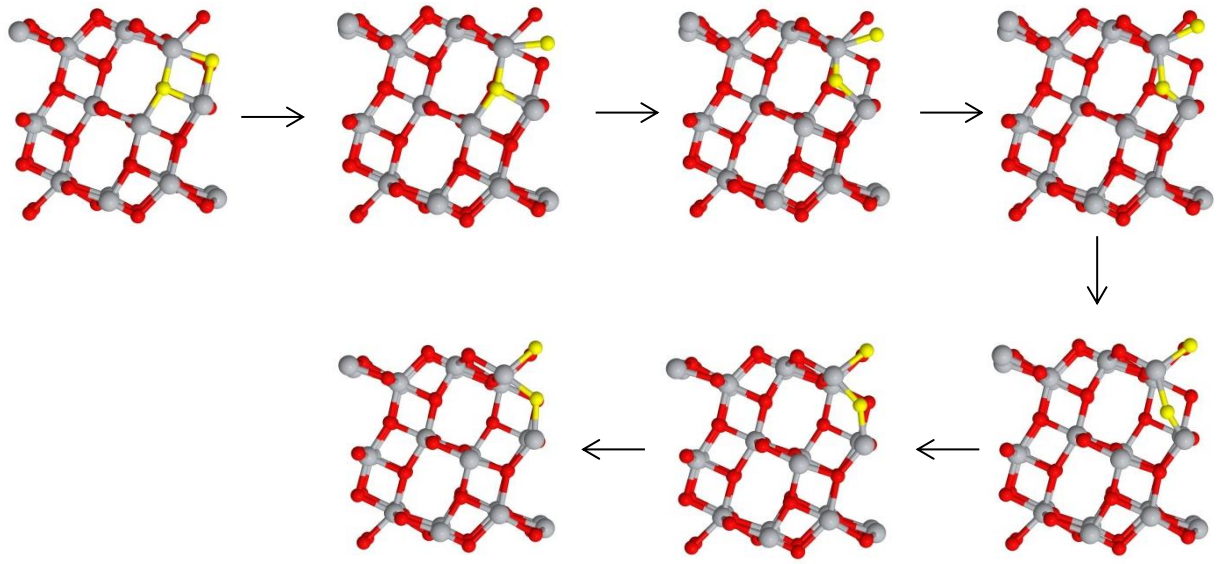

Figure 11: The ReaxFF optimized V_{O1} → V_{O4} pathway (Ti = gray, O = red (dark gray), Moving O = yellow (light gray)).

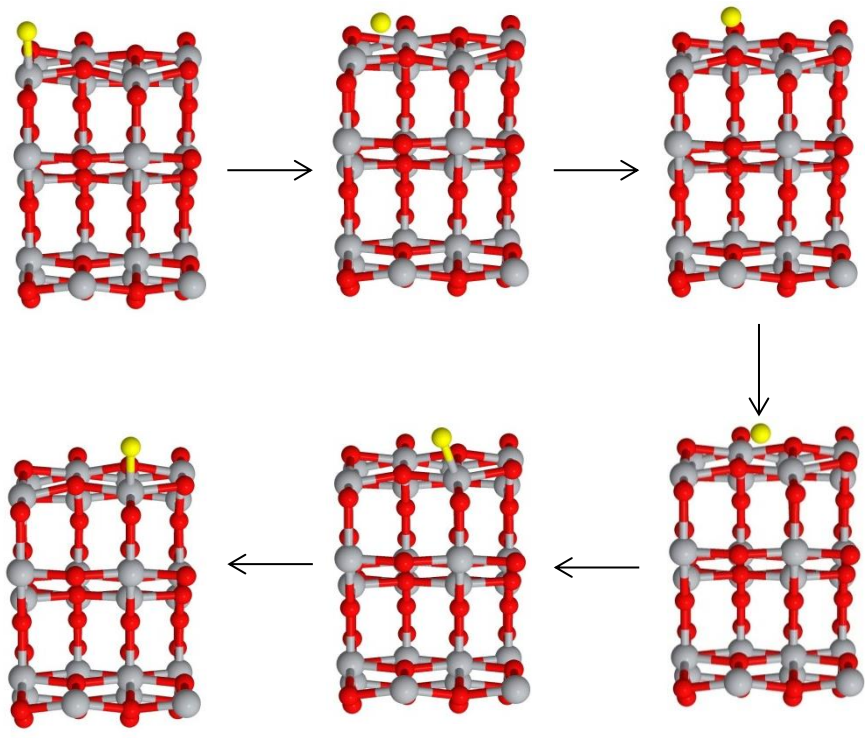

Figure 12: The ReaxFF optimized V_{O1} → $V_{O1`}$ pathway (Ti = gray, O = red (dark gray), Moving O = yellow (light gray)).

3.4 Oxygen adsorption

Molecular oxygen (O_2) plays an important role in many of the TiO_2-based catalytic processes. It is important to gather atomic scale information on the interaction of oxygen with reduced anatase surfaces to gain a better fundamental insight in which factors play an important role in the catalytic processes. The adsorption energies of two O_2 molecules on anatase (101) containing a V_{O4}-vacancy have been added to the training set. [41] The behaviour of molecular adsorption is different for one O_2 molecule and for two O_2 molecules adsorbed at the surface. In the case only one O_2 molecule is adsorbed, it will behave as a peroxide, O_2^{2-}, whereas the adsorbed molecules behave as a superoxide, O_2^-, when two O_2 are adsorbed. [41] Since ReaxFF is a classical force field, it cannot describe both situations, as both structures have a comparable geometry but a different electronic structure. However, the peroxide state will only play a role at very low coverages. Moreover, the superoxide state is also the state found in experimental studies [51,52]. We therefore chose to add the superoxide data and not the peroxide data. It is also found theoretically that it is more favourable by 3.23 kcal/mol to have two O_2 molecules adsorbed than one O_2 adsorbed and one O_2 in the gas phase. [41] This also indicates that the adsorbed O_2 molecule is more stable in its superoxide state than in its peroxide state. The different adsorption sites on an anatase (101) surface consisting of 3 atomic layers and 108 atoms (corresponding to the stoichiometric structure) are indicated in figure 13 and correspond to the same sites as in reference [41]. The ReaxFF, the DFT [41], Monti and Kim data are represented in figure 14. The site combination 1+5 is the most stable one in the ReaxFF and DFT calculations, due to the fact

that in this combination the O_2 molecules are maximally separated and have one O_2 at the closest adsorption site relative to the V_{O4} oxygen vacancy (site 5). The stability of the adsorbed state increases when a molecule is adsorbed closer to the defect. This trend is well reproduced by the force field. It should be noted, however, that the differences in adsorption energies between the most stable site combinations and the least stable are somewhat larger in ReaxFF than in DFT calculations [41]. This will cause a shift in distribution of the adsorbed states at thermodynamic equilibrium on the defected surface. At thermodynamic equilibrium at 300K the relative probability of the adsorption configuration 1+5 is ~100% and ~96%, for ReaxFF and DFT respectively. Since in MD we consider small surfaces with a high concentration of vacancies the most stable configuration will have the main influence on the chemistry. Thermodynamic equilibrium is not reached during the "impact" and adsorption of O_2 on the surface, and therefore also the less stable configurations will be sampled and be accessible for further reactions. Because of the above reasons we consider that the currently developed force field will give a more than adequate description of reactions occurring at the reduced anatase surface.

It is clear that the force field of Monti and Kim cannot describe the trend and the absolute values. They both underestimate the adsorption energies, and the adsorption site combination of 1+2 is the most stable for Monti and 2+6 for Kim. In DFT both combinations are preceded by the combinations 1+5, 2+5 and 4+5. This will influence the adsorption rate and distribution in a significant manner, and therefore the force fields of Kim and Monti are not capable of describing the processes that will occur during the adsorption of O_2 on the reduced anatase surface.

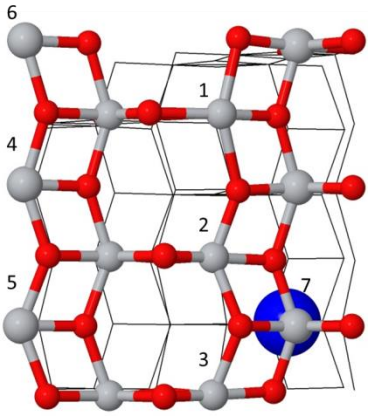

Figure 13: Different adsorption sites of molecular oxygen on a reduced anatase (101) surface containing a V_{O4} vacancy. (Ti = gray, O = red (dark gray), V_{O4} vacancy = blue ball)

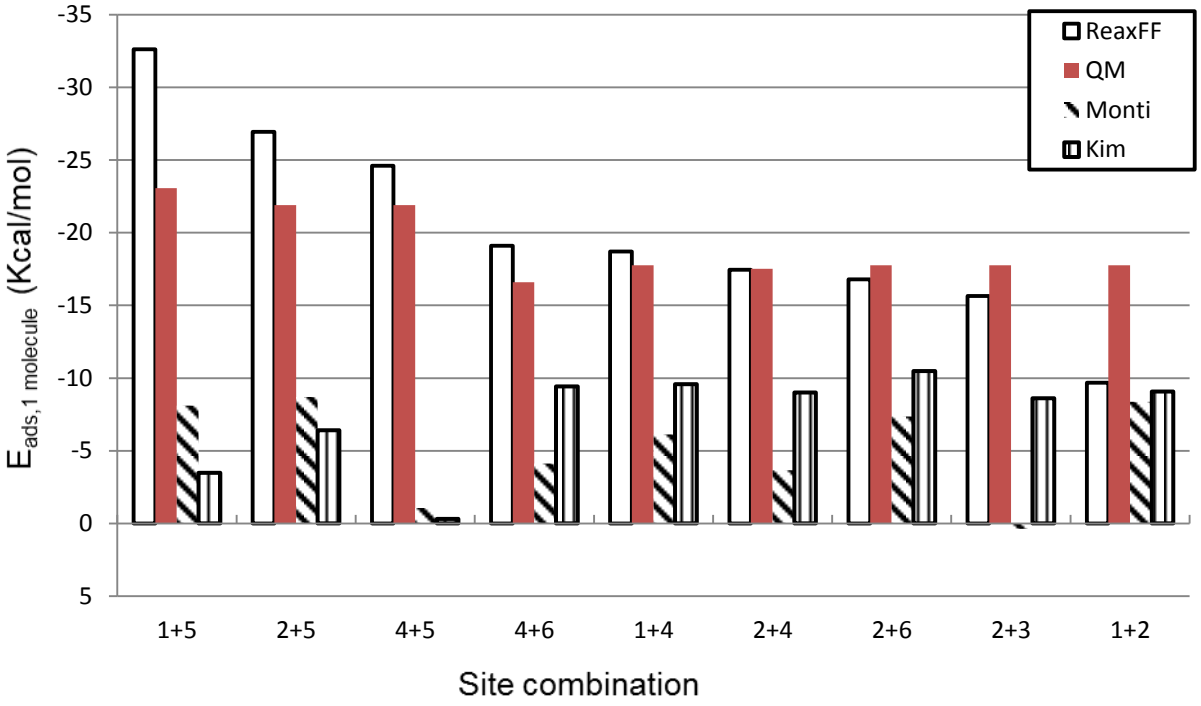

Figure 14: Oxygen adsorption energies per O_2 molecule in various configurations on a reduced anatase (101) surface. [41]

3.5 Application to oxygen vacancy migration

We also applied the developed force field to study the influence of pressure and concentration on the diffusion of the oxygen vacancies on anatase (101) at the surface, $V_{O1} \rightarrow V_{O1`}$, and from the surface to the subsurface, $V_{O1} \rightarrow V_{O4}$. We did not find a significant vacancy concentration dependence on the diffusion barriers for $V_{O1} \rightarrow V_{O1`}$ and $V_{O1} \rightarrow V_{O4}$. A significant influence, on the other hand, was found when the structures were compressed or expanded.

The barrier for diffusion of a V_{O1} vacancy to another $V_{O1´}$ site along [010] at the surface does not decrease when expanding or compressing the structure, as can be seen in figure 15. When the volume is increased the diffusion will be inhibited even stronger. This is caused by the increasing distance between the titanium atoms from the different V_{O1} sites, such that the bonding interaction at the transition state will be lower than in the unexpanded structure and therefore destabilizes the transition state. When compressing the structure the diffusion barrier remains approximately the same up to a compression of 12%. Only after this point the barrier starts to increase.

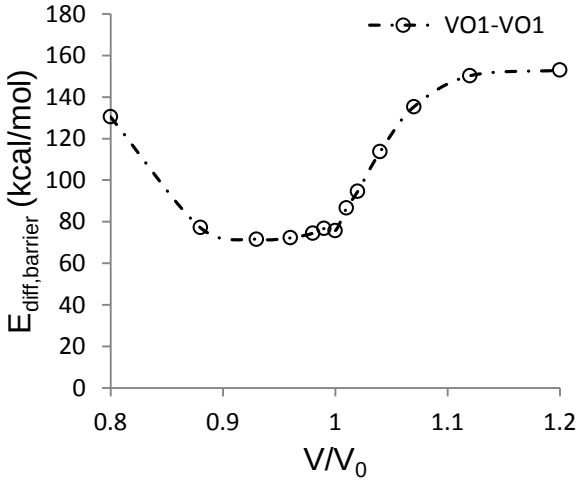

Figure 15: Diffusion energy barriers for the diffusion of a V_{O1} vacancy along the [010] direction on anatase (101) for compressing and expanding the surface.

Figure 16 shows the influence of compressing and expanding the structure on the diffusion barrier of oxygen vacancies from the surface to the subsurface in anatase (101). In this diffusion mechanism we can consider two barriers: One from the direct pathway and one from the reverse pathway. The two pathways correspond to surface-to-subsurface and subsurface-to-surface, respectively. The difference in height of the two barriers is directly related to the difference in stability. When the surface is expanded with about 10% the barriers are approximately equal, and therefore also their stabilities are approximately equal. This indicates that in equilibrium there will be 50% V_{O1} vacancies and 50% V_{O4} vacancies. However, when compressing the structure, the barrier for the subsurface-to-surface pathway is much lower than for the surface-to-subsurface path. Since the barrier from the surface to the subsurface is quite low, equilibrium will be reached rather fast and most vacancies will occur in the subsurface. This will have a large influence on the surface reactivity, because of the different behaviour of subsurface sites compared to the surface sites. When perturbing the structure more than 10-12% expansion or compression, the diffusion will be mainly inhibited.

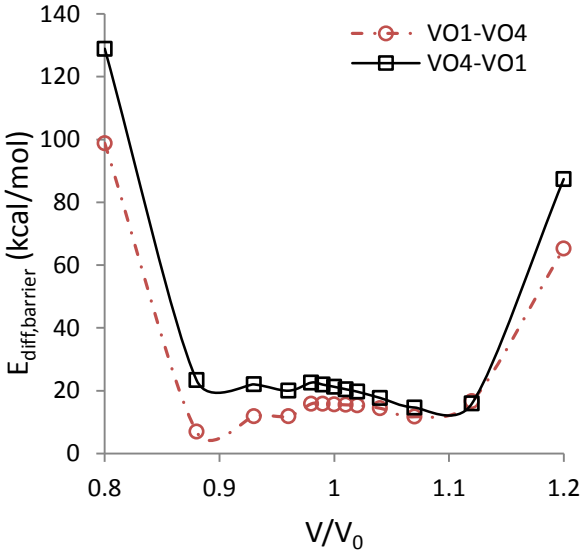

Figure 16: Diffusion energy barriers for the diffusion of a V_{O1} vacancy to a V_{O4} site and the reverse pathway in anatase (101) for compressing and expanding the surface.

Finally, we also studied the possibility of vacancy diffusion in the subsurface, since the diffusion at the surface is mainly inhibited (diffusion energy barrier of 61.12 kcal/mol for V_{O1} → V_{O1}) [7,40]. The minimal energy pathway for the diffusion between two V_{O4} subsurface sites is shown in figure 17. The corresponding energy barrier is 27.7 kcal/mol, which is significantly lower than for the surface diffusion, V_{O1}→$V_{O1`}$ along [010]. The calculated barrier of 27.7 kcal/mol is in the range ~25 kcal/mol – 41 kcal/mol, as estimated for the lateral diffusion energies by Scheiber et al. [53]. It is clear that the lateral redistribution on the surface and in the subsurface will be dominated by diffusion in the subsurface, since also the barriers for diffusion from the surface to the subsurface and vice versa, 17.07 kcal/mol and 21.91 kcal/mol respectively [7,40], are significantly lower than for diffusion on the surface. This is in agreement

with experimental observations of a reduced anatase (101) surface, where surface defects disappear at one position and appear at another position at the same or neighboring rows [53].

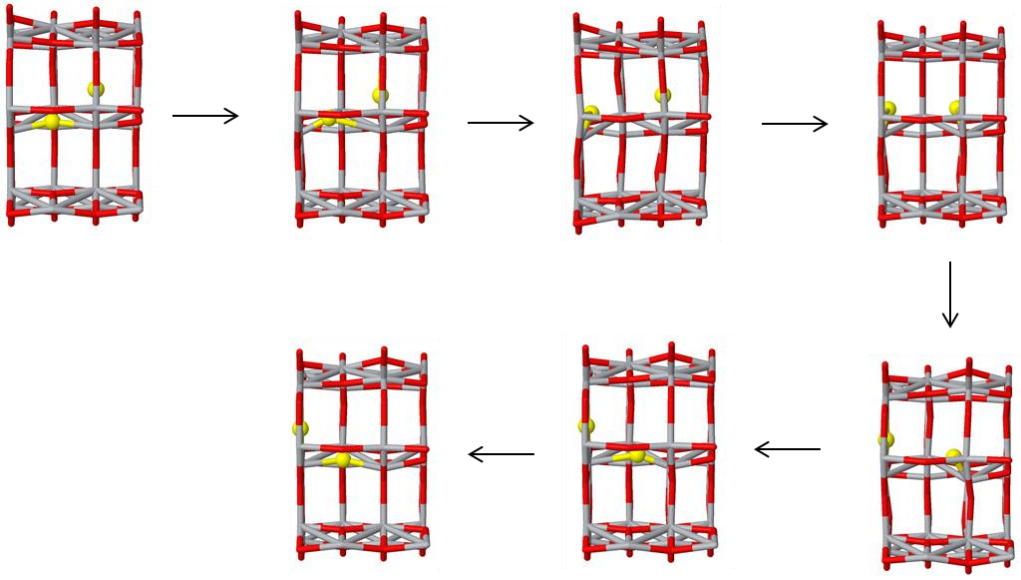

Figure 17: The ReaxFF optimized V_{O4} → $V_{O4`}$ pathway (Ti = gray, O = red (dark gray), Moving O = yellow (light gray))

3.6 Future application of the force field

Using the developed force field, we will also study the growth of titanium dioxide nanocrystals starting from TiO_2 monomers. The TiO_2 monomers are formed during volumetric decomposition and hydrolysis [54] of titanium isopropoxide (TTIP) and are deposited on the surface by direct chemisorption [55] of the gasphase TiO_2. Another reaction that can occur is surface deposition of TiO_2 by TTIP [56], but with the right conditions this reaction can be eliminated from the surface deposition. Indeed, Neyts et al. [57] and Baguer et al. [58] simulated that for atmospheric pressure chemical vapor deposition this reaction stops contributing to the surface deposition at temperatures of 973K or higher in their used set-up. With the simulations on the growth of

titanium dioxide nanocrystals we hope to gain a better insight in the processes occurring during the crystal growth.

4. Conclusions

We developed a ReaxFF reactive force field for studying the influence of intrinsic point defects on the chemistry of TiO_2 condensed-phases. The ReaxFF parameters were fitted against DFT and experimental data to reproduce the equations-of-state, TiO_2-cluster stabilities, defect formation energies, defect diffusion barriers and oxygen adsorption energies. All important data are reproduced quite satisfactory. In comparison with two other recently developed ReaxFF force fields for TiO_2, the current force field represents a significant improvement in the description of the chemistry related to intrinsic point defects. We should however emphasize that these two other force fields were not developed for this purpose and have already been used successfully in other studies relating to different topics. We have applied the developed force field to study the influence of concentration of oxygen vacancies and pressure on the diffusion energy barriers from the surface to the subsurface and on the surface and relative stabilities of the defects on an anatase (101) surface. No significant influence was found for varying the concentration. Compressing or expanding the structure, however, causes a significant redistribution of the surface and subsurface vacancy sites. Also the subsurface oxygen vacancy diffusion barrier was calculated and is found to be consistent with experimental data. The developed force field is able to describe a wide range of effects on the chemistry of the anatase titanium dioxide.

Acknowledgement

Stijn Huygh is funded as aspirant of the Research Foundation Flanders (FWO, Brussels, Belgium). This work was carried out in part using the Turing HPC infrastructure at the CalcUA

core facility of the Universiteit Antwerpen (UA), a division of the Flemish Supercomputer Center VSC, funded by the Hercules Foundation, the Flemish Government (department EWI) and the UA.

Supporting information

Supporting Information Available: The developed force field, formatted as needed for the ReaxFF program, is included in the supporting information.

References

[1] Linsebigler, A. L.; Lu, G.; Yates, J. T. Photocatalysis on TiO2 surfaces – principles, mechanisms, and selected results. J. Chem. Rev. **1995**, 95, 735-758, DOI: 10.1021/cr00035a013.

[2] Grätzel, M. Photoelectrochemical cells. Nature 2001, 414, 338-344, DOI: 10.1038/35054655.

[3] Diebold, U. The surface science of titanium dioxide. Surf. Sci. Rep. **2003**, 48, 53-229, DOI: 10.1016/S0167-5729(02)00100-0.

[4] Henderson, M. A. Surface perspective on self-diffusion in rutile TiO2. Surf. Sci. **1999**, 419, 174-187, DOI: 10.1016/S0039-6028(98)00778-X.

[5] Lazzeri, M.; Vittadini, A.; Selloni, A. Structure and energetics of stoichiometric TiO2 anatase surfaces. Phys. Rev. B **2001**, 63, 155409, DOI: 10.1103/PhysRevB.63.155409

[6] Diebold, U.; Ruzycki, N.; Herman, G. S.; Selloni, A. One step towards bridging the materials gap: surface studies of TiO2 anatase. Catal. Today **2003**, 85, 93-100, DOI: 10.1016/S0920-5861(03)00378-X.

[7] Cheng, H.Z.; Selloni, A. Surface and subsurface oxygen vacancies in anatase TiO2 and differences with rutile. Phys. Rev. B **2009**, 79, 092101, DOI: 10.1103/PhysRevB.79.092101.

[8] Hebenstreit, W.; Ruzycki, N.; Herman, G. S.; Gao, Y.; Diebold, U. Scanning tunneling microscopy investigation of the TiO(2) anatase (101) surface. Phys. Rev. B **2000**, 62, R16334-R16336, DOI: 10.1103/PhysRevB.62.R16334.

[9] He, Y.; Dulub, O.; Cheng, H.; Selloni, A.; Diebold, U. Evidence for the Predominance of Subsurface Defects on Reduced Anatase TiO2(101). Phys. Rev. Lett. **2009**, 102, 106105, DOI: 10.1103/PhysRevLett.102.106105.

[10] Thomas, A. G.; Flavell, W. R.; Mallick, A. K.; Kumarasinghe, A. R.;Tsoutsou, D.; Khan, N.; Chatwin, C.; Rayner, S.; Smith, G. C.; Stockbauer, R. L.; et al. Comparison of the electronic structure of anatase and rutile TiO_2 single-crystal surfaces using resonant photoemission and x-ray absorption spectroscopy. Phys. Rev. B **2007**, 75, 035105-1-12, DOI: 10.1103/PhysRevB.75.035105.

[11] van Duin, A. C. T.; Dasgupta, S.; Lorant, F.; Goddard, W. A. ReaxFF: A reactive force field for hydrocarbons. J. Phys. Chem. A **2001**, 105, 9396-9409, DOI: 10.1021/jp004368u.

[12] Plimton, S.J. Fast parallel algorithms for short-range molecular dynamics. J. Comput. Phys. **1995**, 117, 1-19, DOI: 10.1006/jcph.1995.1039

[13] Nakano, A.; Kalia, R.K.; Nomura, K.; Sharma, A.; Vashishta, P.; et al. A divide-and-conquer/cellular-decompositition framework for million-to-billion atom simulations of chemical reactions. Comput. Mater. Sci. **2007**, 38, 642-652, DOI: 10.1016/j.commatsci.2006.04.012

[14] Nomura, K. I.; Kalia, R. K.; Nakano, A.; Vashishta, P.; van Duin, A. C. T.; Goddard, W. A. Dynamic transition in the structure of an energetic crystal during chemical reactions at shock front prior to detonation. Phys Rev. Lett. **2007**, 99, 148303, DOI: 10.1103/PhysRevLett.99.148303

[15] Chen, H. P.; Kalia, R. K.; Kaxiras, E.; Lu, G.; Nakano, A.; et al. Embrittlement of metal by solute segregation-induced amorphization. Phys. Rev. Lett. **2010**, 104, 155502, DOI: 10.1103/PhysRevLett.104.155502

[16] Zybin, S. V., Goddard, W. A., Xu, P. van Duin, A. C. T., Thomson, A. P. Physical mechanism of anisotropic sensitivity in pentaerythritol tetranitrate from compressive-shear reaction dynamics simulations. Appl. Phys. Lett. **2010**, 96, 081918, DOI: 10.1063/1.3323103

[17] Liang, T.; Devine, B.; Phillpot, S. R.; Sinnot, S. B. Variable charge reactive potential for hydrocarbons to simulate organic-copper interactions. J. Phys. Chem. A **2012**, 116, 7976-7991, DOI: 10.1021/jp212083t

[18] Devine, B. D.; Shan, T.-R.; Cheng, Y.-T.; McGaughey, A.; Lee, M.-Y.; et al. Atomistic simulations of copper oxidation and Cu/Cu_2O interfaces using charge-optimized many-body potentials. Phys. Rev. B **2011**, 84, 125308, DOI: 10.1103/PhysRevB.84.125308

[19] Cheng, Y.-T., Shan, T.-R., Devine, B.; Lee, D.; Liang, T.; et al. Atomistic simulations of the adsorption and migration barriers of Cu adatoms on ZnO surfaces using COMB potentials. Surf. Sci. **2012**, 606, 1280-1288, DOI: 10.1016/j.susc.2012.04.007

[20] Shan, T.-R.; Devine, B. D.; Hawkins, J. M.; Asthagiri, A.; Phillpot, S. R.; Sinnott, S. B. Second-generation charge optimized many-body potential for Si/SiO_2 system and amorphous silica. Phys. Rev. B **2010**, 82, 235302, DOI: 10.1103/PhysRevB.82.235302

[21] Yu, J., Sinnott, S. B.; Phillpot, S. R. Charge optimized many-body potential for the Si/SiO_2 system. Phys. Rev. B **2007**, 75, 085311, DOI: 10.1103/PhysRevB.75.085311

[22] Li, Y.; Shan T.-R.; Liang, T.; Sinnott, S. B.; Phillpot, S. R. Classical interatomic potential for orthorhombic uranium. J. Phys. Condens. Matter. **2012**, 24, 235403, DOI: 10.1088/0953-8984/24/23/235403

[23] Liang, T.; Shin, Y. K.; Cheng, Y.-T.; Yilmaz, D. E.; Vishnu, K. G.; Berners, O.; Zou, C.; Phillpot, S. R.; Sinnott, S. B.; van Duin, A. C. T. Reactive potentials for advanced atomistic simulations. Annu. Rev. Mater. Res. **2013**, 43, 12.1-12.21, DOI: 10.1146/annurev-matsci-071312-121610

[24] Mortier, W. J.; Ghosh, S. K.; Shankar, S. Electronegativity equalization method for the calculation of atomic charges in molecules. J. Am. Chem. Soc. **1986**, 108, 4315-4320, DOI: 10.1021/ja00275a013.

[25] Chenoweth, K.; van Duin, A. C. T.; Goddard, W. A. ReaxFF reactive force field for molecular dynamics simulations of hydrocarbon oxidation. J. Phys. Chem. A **2008**, 112, 1040-1053, DOI: 10.1021/jp709896w.

[26] Raymand, D.; van Duin, A.C.T.; Spangberg, D.; Goddard, W. A.; Hermansson, K. Water adsorption on stepped ZnO surfaces from MD simulation. Surf. Sci. **2010**, 604, 741-752, DOI: 10.1016/j.susc.2009.12.012.

[27] Aryanpour, M.; van Duin, A.C.T.; Kubicki, J. D. Development of a Reactive Force Field for Iron-Oxyhydroxide Systems. J. Phys. Chem. A **2010**, 114, 6298-6307, DOI: 10.1021/jp101332k.

[28] Fogarty, J.C.; Aktulga, H. M.; Grama, A. Y.; van Duin, A. C. T.; Pandit, S. A. A reactive molecular dynamics simulation of the silica-water interface. J. Chem. Phys. **2010**, 132(17), 174704, DOI: 10.1063/1.3407433.

[29] Rahaman, O.; van Duin, A.C.T.; Goddard, W.A., III; Doren, D. J. Development of a ReaxFF Reactive Force Field for Glycine and Application to Solvent Effect and Tautomerization. J. Phys. Chem. B **2011**, 115, 249-261, DOI: 10.1021/jp108642r.

[30] Kim, S.-Y.; Kumar, N.; Persson, P.; Sofo, J.; van Duin, A.C.T.; Kubicki, J. D. Development of a ReaxFF reactive force field for titanium dioxide/water systems. Langmuir **2013**, 29, 7838-7846, DOI: 10.1021/la4006983

[31] Monti, S.; van Duin A.C.T.; Kim, S.-Y.; Barone, V. Exploration of the Conformational and Reactive Dynamics of Glycine and Diglycine on TiO2: Computational Investigations in the Gas Phase and in Solution. J. Phys. Chem. **2012**, 116, 5141-5150, DOI: 10.1021/jp2121593.

[32] Kim, S.-Y.; van Duin, A.C.T.; Kubicki, J. D. Molecular dynamics simulations of the interactions between TiO2 nanoparticles and water with Na+ and Cl-, methanol, and formic acid using a reactive force field. J. Materials Research **2013**, 28, 513-520, DOI: 10.1557/jmr.2012.367.

[33] Muscat, J.; Swamy, V.; Harrison, N. M. First-principles calculations of the phase stability of TiO2. Phys. Rev. B. **2002**, 65, 224112/1-15, DOI: 10.1103/PhysRevB.65.224112.

[34] Beltrán, A.; Gracla, L.; Andrés, J. Density Functional Theory Study of the Brookite Surfaces and Phase Transitions between Natural Titaninia Polymorphs. J. Phys. Chem. B **2006**, 110, 23417-23423, DOI: 10.1021/jp0643000

[35] Ranade, M. R.; Navrotsky, A.; Zhang, H.Z.; Banfield, J. F.; Elder, S.H.; Zaban, A.; Borse, P. H.; Kulkarni, S. K.; Doran, G. S.; Whitfield, H. J. Energetics of nanocrystalline TiO2. Proc. Natl. ACAD. Sci. USA **2002**, 99, 6476-6481, DOI: 10.1073/pnas.251534898.

[36] Cox, J. D.; Wagman, D. D.; Medvedev, V.A., CODATA Key Values for Thermodynamics, Hemisphere Publishing Corp., New York, **1984**, 1

[37] Albaret, T.; Finocchi, F.; Noguera, C. Density functional study of stoichiometric and O-rich titanium oxygen clusters. J. Chem. Phys. **2000**, 113, 2238-2249, DOI: 10.1063/1.482038.

[38] Jeong, K. S.; Chang, C.; Sedlmayr, E.; Sulzle, D. Electronic structure investigation of neutral titanium oxide molecules TixOy. J. Phys. B – At. Mol. Opt. Phys. **2000**, 33, 3417-3430, DOI: 10.1088/0953-4075/33/17/319.

[39] Lundqvist, M. J.; Nilsing, M.; Persson, P.; Lunell, S. DFT study of bare and dye-sensitized TiO2 clusters and nanocrystals. Int. J. Quantum. Chem. **2006**, 106, 3214-3234, DOI: 10.1002/qua.21088.&

[40] Cheng, H. Z.; Selloni, A. Energetics and diffusion of intrinsic surface and subsurface defects on anatase TiO(2)(101). J. Chem. Phys. **2009**, 131, 054703, DOI: 10.1063/1.3194301.

[41] Aschauer, U.; Chen, J.; Selloni, A. Peroxide and superoxide states of adsorbed O-2 on anatase TiO2 (101) with subsurface defects. Phys. Chem. Chem. Phys. **2010**, 12, 12956-12960, DOI: 10.1039/c0cp00116c.

[42] van Duin, A. C. T.; Baas, J. M. A.; van de Graaf, B. Delft Molecular Mechanics – A new approach to hydrocarbon force-fields – inclusion of a geometry-dependent charge calculation. J.Chem. Soc. Faraday Trans. **1994**, 90, 2881-2895, DOI: 10.1039/ft9949002881

[43] Zhu, K.R.; Zhang, M.S.; Hong, J.M.; Tin, Z. Size effect on phase transition sequence of TiO_2 nanocrystal. Mat. Sci. and Eng. A **2005**, 403, 87-93, DOI: 10.1016/j.msea.2005.04.029

[44] Levchenko, A. A.; Li, G.; Boerio-Goates, J.; Woodfield, B. F.; Navrotsky, A. TiO2 stability landscape: Polymorphism, surface energy, and bound water energetics. Chem. Mat. **2006**, 18, 6324-6332, DOI: 10.1021/cm061183c.

[45] Smith, S.J.; Stevens, R.; Liu, S.; Li G.; Navrotsky. A.; Boerio-Goates, J.; Woodfield, B. Heat capacities and thermodynamic functions of TiO_2 anatase and rutile: Analysis of phase stability. Am. Min. **2009**, 94, 2-3, DOI: 10.2138/am.2009.3050

[46] Aschauer, U.; He, Y.; Cheng, H.; Li, S.-C.; Diebold, U.; Selloni, A. Influence of Subsurface Defects on the Surface Reactivity of TiO_2: Water on Anatase (101). J. Phys. Chem. C, **2010**, 114, 1278-1284, DOI: 10.1021/jp910492b

[47] Sorescy, D.C.; Al-Saidi, W. A.; Jordan, K. D. CO_2 adsorption on TiO_2(101) anatase: A dispersion-corrected density functional theory study. J. Chem. Phys. **2011**, 1335, 124701-1-17, DOI: 10.1063/1.3638181

[48] Burdett, J. K.; Hughbanks, T.; Miller, G. J.; Richardson, J. W.; Smith, J. V. Structural electronic relationships in inorganic solids – powder neutron-diffraction studies of the rutile and anatase polymorphs of titanium-dioxide at 15 and 295K. J. Am. Chem. Soc. **1987**, 109, 3639-3646, DOI: 10.1021/ja00246a021

[49] Meagher, E. P.; Lager, G. A. Polyhedral thermal expansion in the TiO2 Polymorphs: refinement of the crystal structures of rutile and brookite at high termperature. Can. Mineral. **1979**, 17, 77-85

[50] Henkelman, G.; Uberuaga, B.P.; Jonsson, H. A climbing image nudged elastic band method for finding saddle points and minimum energy paths. J. Chem. Phys. **2000**, 113, 9901-9904, DOI: 10.1063/1.1329672

[51] Berger, T.; Sterrer, M.; Diwald, O.; Knozinger, E.; Panayotov, D.; Thompson T. L.; Yates, J. T. Light-induced charge separation in anatase TiO2 particles. J. Phys. Chem. B **2005**, 109, 6061-6068, DOI: 10.1021/jp0404293.

[52] Carter, E.; Carley A. F.; Murphy, D. M. Evidence for O-2(-) radical stabilization at surface oxygen vacancies on polycrystalline TiO2. J. Phys. Chem. C **2007**, 111, 10630-10638, DOI: 10.1021/jp0729516.

[53] Scheiber, P.; Fidler, M.; Dulub, O.; Schmid, M.; Diebold, U.; Hou, W.; Aschauer, U.; Selloni, A. (Sub)Surface Mobility of Oxygen Vacancies at the TiO2 Anatase (101) Surface. Phys. Rev. Lett. **2012**, 109, 136103, DOI: 10.1103/PhysRevLett.109.136103.

[54] Okuyama, K.; Ushio, R.; Kousaka, Y.; Flagan, R.C.; Seinfeld, J.H. Particle generation in a chemical vapor deposition process with seed particles, AIChE J. **1990**, 36, 409-419, DOI: 10.1002/aic.690360310.

[55] Lee, H.-Y.; Kim, H.-G. The role of gas-phase nucleation in the preparation of TiO2 films by chemical-vapor-deposition. Thin solid films **1993**, 229, 187-191.

[56] Seto, T.; Shimada, M.; Okuyama, K. Evaluation of sintering of nanometer-sized titania using aerosol method. Aerosol Sci. Technol. **1995**, 23, 183-200, DOI: 10.1080/02786829508965303.

[57] Neyts, E.; Bogaerts, A.; De Meyer, M.; Van Gils, S. Macroscale computer simulations to investigate the chemical vapor deposition of thin metal-oxide films. Surf. & Coatings Technol. **2007**, 201, 8838-8841, DOI: 10.1016/j.surfcoat.2007.04.102.

[58] Baguer, N.; Neyts, E.; Van Gils, S.; Bogaerts, A. Study of Atmospheric MOCVD of TiO_2 thin films by means of Computational Fluid Dynamics Simulations. Chem. Vapor Deposition. **2008**, 14, 339-346, DOI: 10.1002/cvde.200806708